Strain engineering of ZnO thermal conductivity

Juan Antonio Seijas-Bellido,[1] Riccardo Rurali,[1] Jorge Íñiguez,[2,3] Luciano Colombo,[4] and Claudio Melis[4,*]
[1]*Institut de Ciència de Materials de Barcelona (ICMAB–CSIC) Campus de Bellaterra, 08193 Bellaterra, Barcelona, Spain*
[2]*Materials Research and Technology Department, Luxembourg Institute of Science and Technology (LIST), Avenue des Hauts-Fourneaux 5, L-4362 Esch/Alzette, Luxembourg*
[3]*Physics and Materials Science Research Unit, University of Luxembourg, 41 Rue du Brill, L-4422 Belvaux, Luxembourg*
[4]*Department of Physics, University of Cagliari, Cittadella Universitaria, I-09042 Monserrato (Ca), Italy*

(Received 19 February 2019; published 11 June 2019)

Using a combination of equilibrium classical molecular dynamics (within the Green-Kubo formalism) and the Boltzmann transport equation, we study the effect of strain on the ZnO thermal conductivity focusing in particular on the case of hydrostatic and uniaxial strain. The results show that in the case of hydrostatic strain up to ±4%, we can obtain thermal conductivity variations of more than 100%, while for uniaxial strains the calculated thermal conductivity variations are comparatively less pronounced. In particular, by imposing uniaxial compressive strains up to −4%, we estimate a corresponding thermal conductivity variation close to zero. The mode analysis based on the solution of the Boltzmann transport equation shows that for hydrostatic strains, the thermal conductivity variations are mainly due to a corresponding modification of the phonon relaxations times. Finally, we provide evidence that for uniaxial compressive strains the contribution of the phonon relaxations time is balanced by the increase of the group velocities leading to a thermal conductivity almost unaffected by strain.

DOI: 10.1103/PhysRevMaterials.3.065401

I. INTRODUCTION

Strain engineering is an active field of research in condensed matter physics and in nanoscience with several applications in the design and optimization of electronic devices [1–3]. It consists of tuning the properties of a material by a suitable compressive or tensile strain. Indeed, the use of strained Si in conventional electronic devices represented a significant technological breakthrough, dramatically boosting chip speeds because of the increased electronic mobility [4,5].

Comparatively less attention has been devoted to the effect of strain on thermal conduction [6] which is however a key feature for thermoelectric applications, i.e., the conversion of heat into electricity via the Seebeck effect [7]. The physics of thermoelectricity is summarized by the figure of merit $ZT = S^2\sigma/\kappa$ where S is the Seebeck coefficient, while σ and κ are the electrical and thermal conductivity, respectively. High ZT values can be therefore obtained by reducing the thermal conductivity while preserving good charge transport characteristics or alternatively, by optimizing charge transport without simultaneously increasing the thermal conductivity. In this perspective ZnO is considered a promising material for thermoelectric conversions [8] due to its low cost, stability at high temperature, and mainly because of its excellent charge carrier transport properties [9,10]. The maximum ZT measured up to now for Al-doped ZnO is as small as 0.3 at $T = 1000$ K [8], which is still far below the expected ZT values of ∼1 of most commercial thermoelectric materials. One of the main issues limiting the figure of merit of ZnO is its intrinsically high thermal conductivity [11]. For this reason it is interesting to investigate the possibility of reducing this feature by strain without affecting the power factor ($S^2\sigma$) or, alternatively, increasing the power factor leaving the corresponding thermal conductivity unchanged. These strategies have been successfully applied to many different materials [12–15].

An overview of the available experiments on the thermal conductivity of solids and liquids under pressure can be found in the paper by Ross *et al.* [16]. The data for covalent semiconducting and insulating materials are relatively scarce and are limited to some polymorphs of SiO_2 [17–19], Si [11], Ge [11], InSb [20], PbTe [21], and a few other compounds. The general trend outlined by these experiments seem to be that κ increases with pressure. However, the fact that the pressure range often differs from one experiment to the other, or that sometimes only data referring to uniaxial stresses are available, have prevented the formulation of a unifying picture on the strain effects on thermal conduction.

The advent of nanowires [22,23], filamentary crystals with diameters in the range of a few to several tens of nanometers, marked an increased interest in the design of materials with tailor made properties via strain engineering. Indeed, values of tensile strain much larger than those achievable in bulk materials have been obtained by a few groups [24–26]. ZnO can be synthesized under several different nanostructured forms and its great potential in several applications, ranging from nanogenerators [27], self-powered devices [28], and strain sensors [29] has been reported. Nevertheless, also in the case of ZnO the effect of strain on the vibrational and thermal properties has seldom been addressed.

Motivated by the above state of affairs, we carry out equilibrium molecular dynamics (EMD) calculations within the

*claudio.melis@dsf.unica.it

Green-Kubo formalism to assess the thermal conductivity of ZnO under strain engineering. Specifically, we study the case of hydrostatic pressure, i.e., homogenous strain, as well as uniaxial strain. Our results show that, in the case of hydrostatic strain, thermal conductivity variations of up to ∼100% can be obtained, while for uniaxial strain they are found to be very small. In particular, we observe that the thermal conductivity variation is almost negligible in the case of uniaxial compressive strains. We also carry out lattice dynamics calculations solving numerically the Boltzmann transport equation (BTE) within the relaxation time approximation (RTA) to rationalize the results of the EMD calculations. This analysis shows that, in the case of hydrostatic strain, the thermal conductivity variation is mainly due to a corresponding modification of the phonon relaxations times. On the other side, in the case of uniaxial compressive strain the contribution of the phonon relaxation time is balanced by the increase of their group velocity, leading to a thermal conductivity essentially identical to the unstrained case.

II. METHODS

A. Buckingham potential

The ZnO wurtzite phase was described by the sum of a Coulomb and a Buckingham-type two-body potential of the form

$$U(r_{ij}) = \frac{q_i q_j}{4\pi\epsilon_0 r_{ij}} + A\exp\left(-\frac{r_{ij}}{\rho}\right) - \frac{C}{r_{ij}^6}, \tag{1}$$

which has been extensively used for metal oxides [30]. Here q_i and q_j are the charges of atoms i and j while r_{ij} is their relative distance. The first term describes the long-range Coulomb interactions, the second term is a short-range repulsion potential, and the third term is the van der Waals attraction. The parameters A, ρ, and C and all the atomic charges q_i were taken from Ref. [31]. The lattice parameters $a = b = 3.25$ Å and $c = 5.15$ Å of the ZnO wurtzite crystal structure (see Fig. 1) calculated according to the present model are in fairly good agreement with the experimental values [32] (errors are within 1.5 % for both a and c).

B. Equilibrium molecular dynamics

Thermal conductivity κ has been estimated along the a and c crystallographic directions (see Fig. 1) using the Green-Kubo formalism [33]

$$\kappa_{ij} = \frac{V}{k_B T^2}\int_0^t \langle J_i(t) J_j(0)\rangle d\tau, \tag{2}$$

where V is the volume of the system, k_B is the Boltzmann constant, T is the temperature of the system, t is the correlation time, i, j are lattice directions, and the angular brackets denote ensemble averages. The heat flux was sampled according to its standard definition for a pair potential interaction [34].

$$\boldsymbol{J} = \frac{1}{V}\left[\sum_{i=1}^{N}\epsilon_i \boldsymbol{v}_i + \sum_{i=1}^{N}\boldsymbol{r}_i(\boldsymbol{F}_i\cdot\boldsymbol{v}_i) - \frac{1}{2}\sum_{i=1}^{N}\sum_{j\neq i}\boldsymbol{r}_{ij}(\boldsymbol{F}_{ij}\cdot\boldsymbol{v}_i)\right], \tag{3}$$

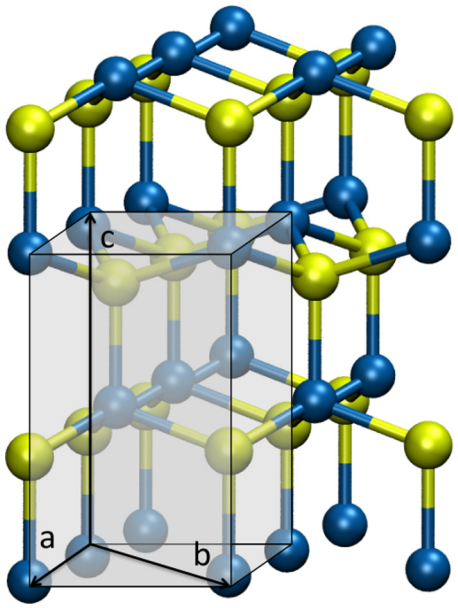

FIG. 1. Stick and ball representation of ZnO wurtzite crystal structure.

where ϵ_i, $\boldsymbol{r}_i$, $\boldsymbol{v}_i$, and $\boldsymbol{v}_i$, are respectively, the total energy, the position, and the velocity of the ith atom, $\boldsymbol{F}_i$ is the force acting over the ith atom, and $\boldsymbol{r}_{ij}$ and $\boldsymbol{F}_{ij}$ are, respectively, the distance and the force between a pair of atoms. In order to estimate the thermal conductivity along the the c (a) crystallographic directions κ_{cc} (κ_{aa}), we sampled the autocorrelation function between the c (a) components of the heat current vector.

The Green-Kubo integral was calculated in a simulation cell with dimensions of $3.859 \times 3.899 \times 4.123\,\mathrm{nm}^3$ containing 5376 atoms. As previously shown for different systems including metal oxides [35–37], such cell dimensions guarantee the lack of any size artifacts that might affect thermal conductivity calculations within the Green-Kubo approach. The sample was preliminarily equilibrated for 500 ps in the isothermal-isobaric (NPT) ensemble, with a timestep of 1 fs, using the Nosé-Hoover thermostat and barostat at temperature and pressures of 300 K and 1 Atm, respectively. The autocorrelation function was then sampled during a 2-ns-long microcanonical simulation. The maximum value chosen for the correlation time was 80 ps. The present choice of the simulation time as well as the maximum correlation time were motivated by the requirement to mitigate as much as possible the statistical error occurring in the estimation of the heat current autocorrelation function, while preserving a reasonable computational cost (more details in the results discussion).

C. Boltzmann transport equation in the relaxation time approximation

We further analyze thermal transport along the c crystallographic direction by means of the Boltzmann transport equation (BTE) in the relaxation time approximation (RTA) [33] as implemented in the ShengBTE code [38]. In this approximation

the thermal conductivity can be written as

$$\kappa = \sum_{\lambda} \kappa_{\lambda} = \frac{1}{N\Omega k_B T^2} \sum_{\lambda} f_{\lambda}(f_{\lambda}+1)(h\nu_{\lambda})^2 v_{\lambda}^2 \tau_{\lambda}, \quad (4)$$

where Ω is the volume of the unit cell, N the number of $\vec{q}$ points, T the temperature, and h the Planck's constant. The index λ encompasses both $\vec{q}$ point and phonon band. f_{λ} is the equilibrium Bose-Einstein distribution function, while ν_{λ}, v_{λ}, and τ_{λ} are, respectively, the frequency, group velocity, and average lifetime of phonon λ. Phonon frequencies ν_{λ} were obtained by finite differences, using the PHONOPY simulation package [39]. We use a ~5.5 Å cutoff for the generation of displacements in the third order force constants matrix of 12 neighbors.

D. Estimation of the Seebeck coefficient

In order to estimate the effect of uniaxial strains on the ZnO Seebeck coefficient, we combine first-principles calculations with the Boltzmann transport theory within the constant scattering time approximation. In detail, we performed density functional theory (DFT) calculations on a wurtzite ZnO four-atom cell using the QUANTUM ESPRESSO package [40,41] and the GGA-PBE [42] exchange-correlation functional plus U (DFT + U) [43]. To describe the electronic structures more accurately, we adopted the DFT + Ud + Up method [44], in which the Ud value for Zn-3d and the Up value for O-2p orbitals were set at 10 and 7 eV, respectively [45]. The Monkhorst-Pack scheme [46] K-points grid sampling in the supercells was set at 12 × 12 × 12. Electron-ion interactions were modeled using the ultrasoft pseudopotential method [47]. The electron wave functions were expanded in plane waves with an energy cutoff of 60 Ry. Using the present computational setup we estimated an electronic ZnO direct band gap of 3.1 eV which is in very good agreement with experimental measurements [48]. The Seebeck coefficient of ZnO was calculated within the Boltzmann transport equation within the constant scattering time approximation using the BOLTZTRAP code [49] and 2222 K points in the Brillouin zone.

III. RESULTS

A. Thermal conductivity of unstrained ZnO

Figure 2 shows the room temperature normalized heat current autocorrelation function (top) and the corresponding thermal conductivity (bottom) as a function of the correlation time for a single trajectory collected for an unstrained bulk ZnO sample. We observe an oscillatory behavior of the heat current autocorrelation function which has been recently also reported for complex silica structures [50,51] and attributed to the relative motion of bonded atoms with different masses [36] or to the presence of optical phonons [52]. Due to the presence of such large oscillations in the autocorrelation function, the direct estimate of the thermal conductivity with the Green-Kubo integral is clearly not trivial since the large amount of noise prevents the identification of a convergence region. A possible strategy recently proposed to directly address the thermal conductivity [50] in this case consists of performing a running average of the integral in overlapping blocks of a few

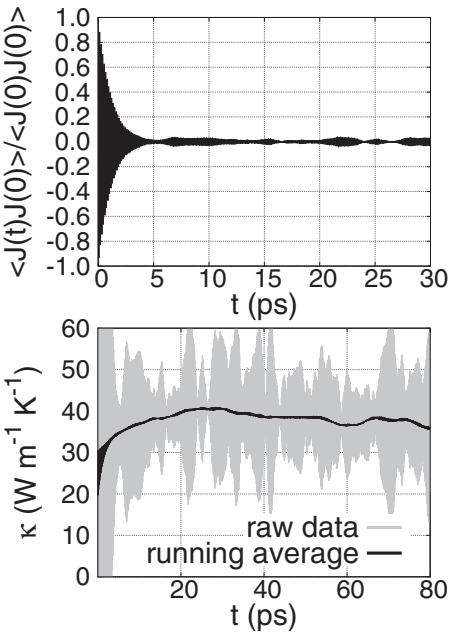

FIG. 2. Room temperature heat current autocorrelation function (up) and the corresponding thermal conductivity κ_{cc} (down) as a function of the correlation time obtained for one single trajectory.

thousands steps. When the convergence region is eventually identified, a time lapse of at least 50 000 time steps is set, over which the integral shows a constant value. In order to improve the statistics, a configurational average over five independent trajectories differentiated by random initial velocities has been performed (see Fig. 3). The error in the average thermal conductivity has been estimated as the corresponding standard deviation.

The estimated value of the thermal conductivity calculated along the c direction is $\kappa_{cc} = 42 \pm 7$ W m^{-1} K^{-1} while in the case of the a direction we obtain $\kappa_{aa} = 38 \pm 6$ W m^{-1} K^{-1}.These two values are in remarkably good agreement with the experimental values, which range between 37 and 47 W m^{-1} K^{-1} [53]. We attribute this satisfactory result to the remarkable accurate description of the acoustic phonon branches provided by the Buckingham-type force field.

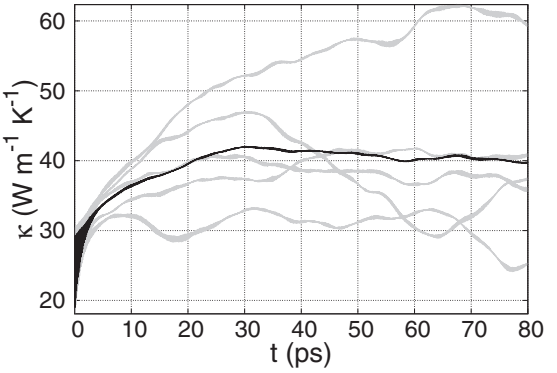

FIG. 3. Room temperature thermal conductivity κ_{cc} as a function of the correlation time for five independent simulations (gray curves) together with the corresponding average (black curve).

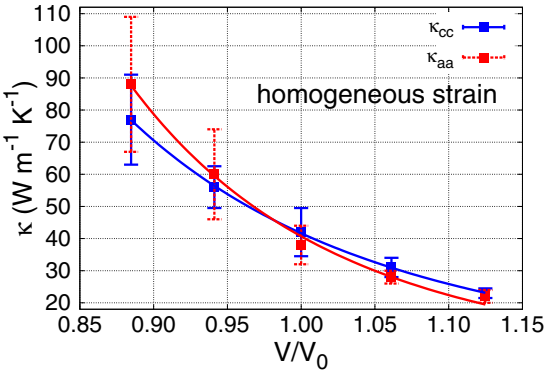

FIG. 4. Room temperature thermal conductivities κ_{cc} (blue) and κ_{aa} (red) as a function of the applied homogeneous strain. The blue and red curves represent the fitting function of Eq. (6) for κ_{cc} and κ_{aa}, respectively.

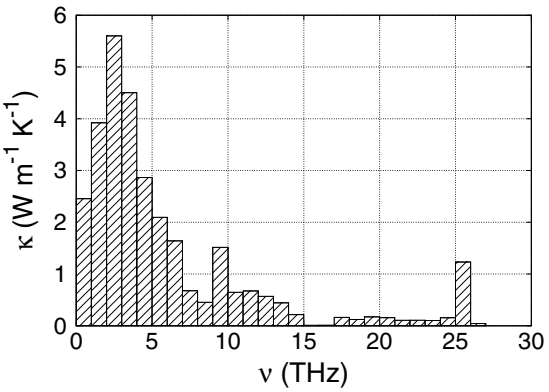

FIG. 5. Spectral contribution to thermal conductivity in the case of the unstrained system at $T = 300$ K.

B. Thermal conductivity of ZnO under hydrostatic strain

We investigated the effect of strain on ZnO thermal conductivity by considering first the case of hydrostatic strain ϵ defined with respect to the equilibrium volume V_0 as:

$$\epsilon = \frac{V}{V_0}, \tag{5}$$

where V is the volume of the strained simulation cell. We applied strains in the interval $\pm 4\%$ by considering steps of 2%. In detail, starting from the unstrained zero pressure cell volume V_0, strain is applied to the atomistic simulation cell by rescaling the size of the periodic box to $V = \epsilon V_0$. Furthermore, the positions of all atoms in the box were also rescaled accordingly. The system was then equilibrated at $T = 300$ K by performing an isothermal simulation as long as 0.5 ns in order to fully relax the atomic positions. The thermal conductivity was then estimated over five different trajectories using the same procedure as described above.

It has been demonstrated [54] that the effect of hydrostatic strain on the thermal conductivity of a crystalline system can be cast in the following power law:

$$\kappa \sim \epsilon^{-\gamma}, \tag{6}$$

where γ is a material dependent parameter. Such a power law has been interpreted as mainly due to the effect of both phonon relaxation time τ and group velocities v_g which show, in turn, the same power-law dependence on the applied hydrostatic strain:

$$\tau \sim \epsilon^{-(2\alpha+2\beta)} \tag{7}$$

and

$$v_g \sim \epsilon^{-\alpha}, \tag{8}$$

where $\gamma = 4\alpha + 2\beta$ and both α and β are material dependent parameters.

Figure 4 shows the thermal conductivities κ_{cc} (blue) and κ_{aa} (red) as a function of strain that we obtained from the Green-Kubo simulations. We observe a very good agreement between the model of Eq. (6) and our data that can be closely fitted as $\kappa_{cc} = 41.65 \times \epsilon^{-5.00}$ (blue curve in Fig. 4) and $\kappa_{aa} = 40.70 \times \epsilon^{-6.26}$ (red curve in Fig. 4).

The present results stand for the reliability of our simulation protocol to describe the thermal conductivity dependence of crystalline systems under hydrostatic strain. We observe that by applying hydrostatic strains up to $+4\%$ (-4%) we are able to decrease (increase) the ZnO thermal conductivity by almost a factor 2 and, therefore, to largely affect its figure of merit. We observe that recent DFT results [55] give a less pronounced dependence of the thermal conductivity with the hydrostatic strain, a fact most likely due to the limitations of the interatomic potential here employed. Nevertheless, the trend is similar to what was found in the present work.

We take profit of the mode analysis offered by the RTA-BTE method to investigate how strain differently affects phonon group velocities and relaxation times. We focus on the two extreme cases of $+4\%$ and -4% strain where any possible effect is expected to be the largest, and we restrict these calculations to the c direction. We preliminary remark that RTA-BTE calculations underestimate κ both for the unstrained case (for which we get $\kappa_{\text{RTA-BTE}} = 30.7$ W m^{-1} K^{-1}) and for the $+4\%$ ($\kappa_{\text{RTA-BTE}} = 9.5$ W m^{-1} K^{-1}) and -4% ($\kappa_{\text{RTA-BTE}} = 60.3$ W m^{-1} K^{-1}) cases. However, the overall thermal conductivity variations with respect to the unstrained case are very similar. Here we address relative variations rather than absolute ones.

Figure 5 shows the spectral contribution to thermal conductivity in the case of the unstrained system. We observe that the main contribution to thermal conductivity is due to phonons at relatively low frequency below 15 THz. A similar behavior has been previously predicted for ZnO in Ref. [53] where it was demonstrated that the thermal conductivity was mainly governed by the six lower phonon branches. This result allows neglecting the contribution of higher frequency modes.

To better understand the effect of the strain we use a technique previously introduced by some of us in Ref. [56]. It is easy to prove that the difference of a product of three magnitudes (hereafter referred to as A, B, and C) in two different situations is given by

$$ABC - A^0B^0C^0 = (A - A^0)B^0C^0 + A^0(B - B^0)C^0 + A^0B^0(C - C^0) + \mathcal{R}, \tag{9}$$

where $\mathcal{R}$ would include all the terms that contain the deviation of two or three magnitudes with respect to the reference situation labeled by the superscript "0," like

$$\mathcal{R} = (A - A^0)(B - B^0)C^0 + \cdots + (A - A^0)(B - B^0)(C - C^0). \quad (10)$$

In this paper, the superscript "0" will indicate zero-strain quantities, while the magnitudes without superscript are for the strained cases. We also define $\Delta g = g - g^0$ for any magnitude g. Using the definition of the thermal conductivity that appears in Eq. (4), this technique allows us to detect the change of which magnitude is more relevant for the global change of the thermal conductivity when we apply strain to the system.

In detail, we group all the terms that are explicitly dependent on the phonon frequencies that appear in Eq. (4) by introducing the quantity $\theta_\lambda = f_\lambda(f_\lambda + 1)v_\lambda^2$, i.e., the frequency-dependent contribution of the specific heat. This allows us to derive the strain-induced variation of κ as

$$\Delta\kappa = \kappa - \kappa^0 = \sum_\lambda \Delta\kappa_\lambda = \frac{h^2}{N\Omega T^2}\sum_\lambda \left[\Delta\left(\frac{1}{V}\right)\theta_\lambda^0 (v_\lambda^0)^2\tau_\lambda^0 + \frac{1}{V_0}\Delta\theta_\lambda (v_\lambda^0)^2\tau_\lambda^0 + \frac{1}{V^0}\theta_\lambda^0\Delta v_\lambda^2\tau_\lambda^0 + \frac{1}{V_0}\theta_\lambda^0 (v_\lambda^0)^2\Delta\tau_\lambda + \mathcal{R}_\lambda\right], \quad (11)$$

where we have applied the mathematical reasoning appearing in Eq. (9). Also in this case we only take into account the c component of all the vector quantities in Eq. (11). This expression allows us to readily identify changes in κ that are dominated by the change of just one of the four factors (V, θ_λ, v_λ, τ_λ) involved in the mode conductivity, while R_λ captures any lingering changes, i.e., changes in κ where the change of two or more factors is implicated.

Figure 6 shows the variations with respect to the unstrained condition of the different contributions to thermal conductivity [see Eq. (11)] in the case of -4% (top) and $(+4\%)$ strains. The largest variation observed in both cases is found for the phonon relaxation times τ_λ (blue dashes), which is predominant with respect to all the other contributions including the group velocities v_λ. Notice that the term $\mathcal{R}_\lambda$ adds to the global trend for negative strains, while for positive strains it has an opposite behavior. This explains why when compressing the material the thermal conductivity increases more than what the thermal conductivity is reduced when expanding it.

C. Thermal conductivity of ZnO under uniaxial strain

We further analyze the effect of strain on the ZnO thermal conductivity by taking into account the uniaxial tensile strain $\eta = (L - L_0)/L_0$, where L is the simulation cell length upon the application of the strain and L_0 is the one corresponding to 0% strain. In detail, the tensile strain was applied along the c direction (see Fig. 1) in the interval $\pm 4\%$ by considering steps of 2%. We focus on the c axis since this is the most common growth orientation of ZnO nanowires and, therefore, it is the crystallographic axis along which high strain can be more easily applied. In this case, upon the elongation of the simulation cell, we perform an NPT (500 ps) simulation by fixing the simulation cell length along the c direction and allowing a full relaxation in the other two directions. The results are shown in Fig. 7. Differently from the previous case, we observe comparatively smaller variations upon the application of the uniaxial strain. In particular, the estimated κ_{aa} values for the 0% and the -4% strain are almost identical indicating a negligible dependence of the thermal conductivity on compressive strains. In order to further validate this result, we estimated the thermal conductivity solving the RTA-BTE for the case of $+4\%$ and -4% uniaxial strains.

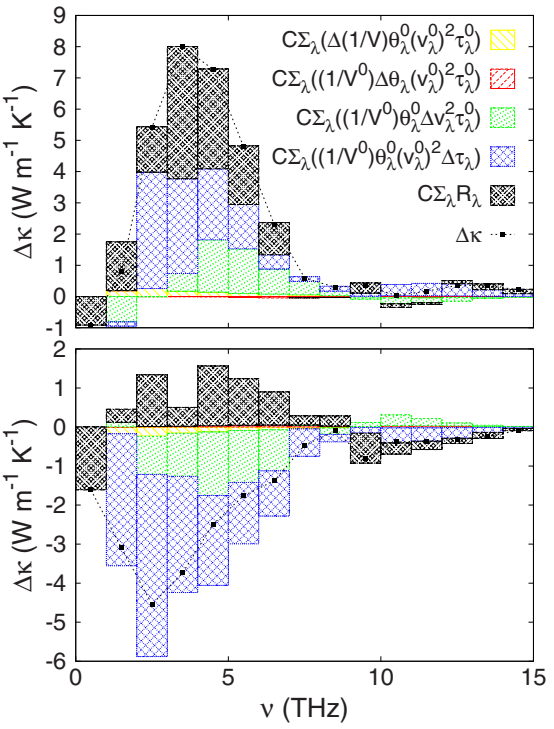

FIG. 6. Differences with respect to the unstrained condition of the different contributions to thermal conductivity [see Eq. (11)] in the case of -4% (top) and $+4\%$ (bottom) hydrostatic strains. The points represent the whole thermal conductivity difference while the colored stripes represents the different contributions.

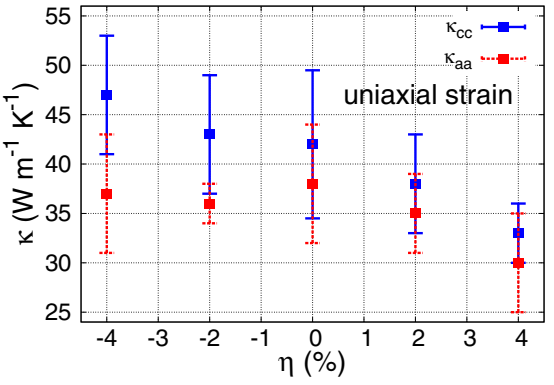

FIG. 7. Room temperature thermal conductivities κ_{cc} (blue) and κ_{aa} (red) as a function of the applied uniaxial strain.

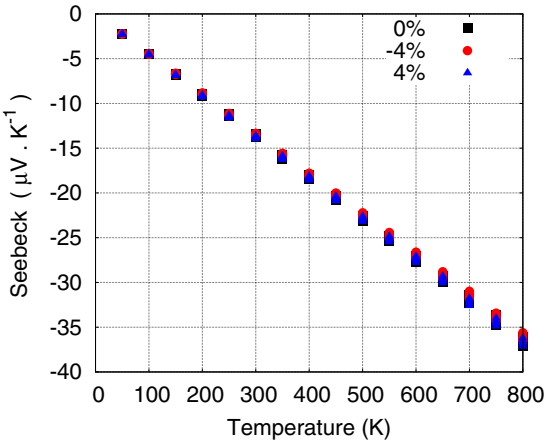

FIG. 8. Temperature dependence of the Seebeck coefficient in the case of 0% (black squares), −4% (red circles), and +4% (blue diamonds) uniaxial strain.

Also in this case, we observe that the thermal conductivities corresponding to the 0% and −4% strain are very similar (30.7 and 30.0 W m^{-1} K^{-1}, respectively), while the κ value corresponding to the 4% strain shows a larger variation being equal to 18.2 W m^{-1} K^{-1}. This agreement between EMD and BTE is particularly remarkable and vouches for the reliability of the results obtained. On one hand, the BTE results indicate that the EMD runs do not suffer from possible shortcomings of this kind of simulations, such as not long enough simulation and correlation times or too small computational cells; on the other hand, the EMD results, which account for anharmonicity at all orders, validate the results obtained from the solution of the BTE where these effects are considered only up to the third order.

We argue that the present result is relevant for thermoelectric applications since it has been reported [57] that the ZnO thin film electrical resistivity can be reduced by more than a factor 4 by imposing a uniaxial (compressive) strain as small as −0.4%. In order to estimate the effect of tensile and compressive uniaxial strains on the ZnO Seebeck coefficient, we performed a set of first principles DFT calculations combined with the Boltzmann transport theory within the constant scattering time approximation. Figure 8 shows the Seebeck coefficient as a function of temperature at a fixed electron carrier concentration of 6×10^{20} cm^{-3} corresponding to the maximum electron concentration achievable in ZnO via doping [8]. Figure 8 clearly shows that the Seebeck coefficient is nearly unaffected by strain over a wide range of temperatures. This allows us to combine three separate results, namely: (i) our calculation indicates that the thermal conductivity is only marginally affected by compressive tensile strain up to 4%; (ii) experimental evidence shows instead that electrical conductivity can be dramatically increased by imposing uniaxial compressive strains; (iii) present first principles calculations show that the Seebeck coefficient is nearly unaffected by tensile strain. This implies the power factor ($S^2\sigma$) as a whole should increase upon uniaxial strain, leading to a corresponding ZT increase.

Similarly to the previous case, we show in Fig. 9 the variations with respect to the unstrained condition of the

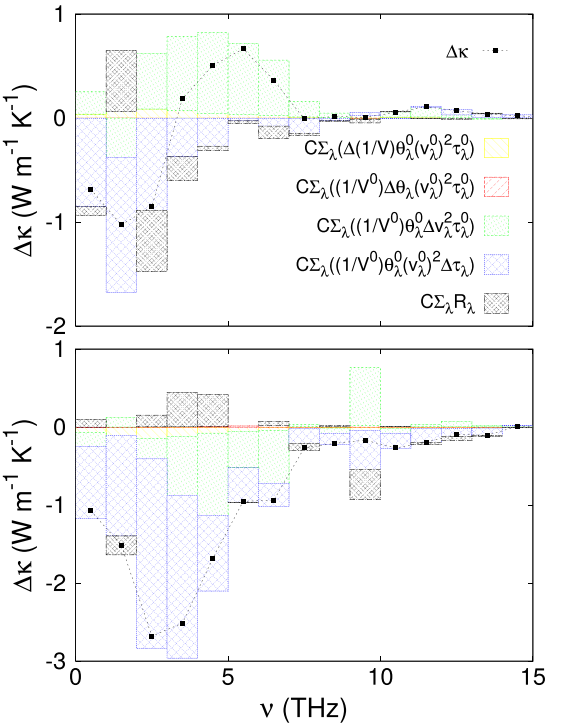

FIG. 9. Differences with respect to the unstrained condition of the different contributions to thermal conductivity [see Eq. (11)] in the case of −4% (top) and +4% (bottom) uniaxial strains. The points represent the whole thermal conductivity difference while the colored stripes represents the different contributions.

different contributions to thermal conductivity in the case of −4% (top) and (+4%) uniaxial strains. We observe large differences with respect to the case of hydrostatic strain. In the case of the −4% strain the detrimental contribution due to the phonon relaxation times at frequencies below ∼3 THz is balanced by the increase of the group velocities (green dashes) at higher frequencies, leading to an overall thermal conductivity equal to the one at 0% strain. On the other side, in the case of 4% strain, the contribution of both phonon relaxation times and group velocities is detrimental, leading to a thermal conductivity reduction with respect to the 0% strain case. A similar competitive mechanism has been recently identified for different telluride systems [58]. Differently from the case of hydrostatic strain, the contribution of the term $\mathcal{R}_\lambda$ (black dashes) is negligible. In order to verify whether the effect of the group velocities is compensated by the effect of the phonon density of states (PDOS), we compared the PDOS in the case of uniaxial compressive and tensile strains with the 0% strain case. In both cases we did not observe any significant PDOS variation, both in the acoustic as well as optical region, with respect to the unstrained sample. For this reason, we cannot claim any compensation effect on the group velocities by corresponding PDOS variation upon the application of tensile strains.

IV. CONCLUSIONS

We have investigated the effect of strain (hydrostatic and uniaxial) on bulk ZnO thermal conductivity using EMD

simulations within the Green-Kubo formalism and the numerical solution of the BTE equation within the RTA approximation. In the case of hydrostatic strain up to ±4% we estimate a corresponding thermal conductivity variation of more than a factor 2. On the other side, for uniaxial strains, the estimated thermal conductivity variations are comparatively very limited. In particular, for uniaxial compressive strain up to −4%, we estimate a negligible thermal conductivity variation. This result is potentially important for thermoelectric applications since the ZnO electrical resistivity is dramatically affected by a uniaxial compressive strain. This would arguably lead to a ZT increase due to the fact that the thermal conductivity would be unaffected. The spectral analysis of the solution of the BTE shows that, for hydrostatic strains, the thermal conductivity variations mainly originate from the variation of the phonon relaxations times. For uniaxial compressive strains instead the contribution of the phonon relaxations time is balanced by the increase of the group velocities.

ACKNOWLEDGMENTS

C.M. and L.C. acknowledge financial support by Fondazione di Sardegna through Progetto biennale di Ateneo 2016 *Multiphysics approach to thermoelectricity*. R.R. and J.A.S.-B. acknowledge financial support by the Ministerio de Economía, Industria y Competitividad (MINECO) under Grant No. FEDER-MAT2017-90024-P and the Severo Ochoa Centres of Excellence Program under Grant No. SEV-2015-0496 and by the Generalitat de Catalunya under Grant No. 2017 SGR 1506. J.Í. thanks the funding of the Luxembourg National Research Fund (Grant No. NR/P12/4853155 COFERMAT).

[1] J. A. Del Alamo, Nature (London) **479**, 317 (2011).
[2] V. M. Pereira and A. C. Neto, Phys. Rev. Lett. **103**, 046801 (2009).
[3] H. J. Conley, B. Wang, J. I. Ziegler, R. F. Haglund, S. T. Pantelides, and K. I. Bolotin, Nano Lett. **13**, 3626 (2013).
[4] J. Hoyt, H. Nayfeh, S. Eguchi, I. Aberg, G. Xia, T. Drake, E. Fitzgerald, and D. Antoniadis, in *Electron Devices Meeting, 2002. IEDM'02. International* (IEEE, 2002), pp. 23–26.
[5] S. I. Association *et al.*, http://www.itrs.net/ (2006).
[6] Y. Han, J.-Y. Yang, and M. Hu, Nanoscale **10**, 5229 (2018).
[7] D. K. C. MacDonald, *Thermoelectricity: An Introduction to the Principles* (Dover Publications Inc., Mineola, NY, 2006).
[8] T. Tsubota, M. Ohtaki, K. Eguchi, and H. Arai, J. Mater. Chem. **7**, 85 (1997).
[9] R. S. Thompson, D. Li, C. M. Witte, and J. G. Lu, Nano Lett. **9**, 3991 (2009).
[10] M. Zhou, H. Zhu, Y. Jiao, Y. Rao, S. Hark, Y. Liu, L. Peng, and Q. Li, J. Phys. Chem. C **113**, 8945 (2009).
[11] P. I. Baranskii, P. P. Kogutyuk, and V. V. Savyak, Sov. Phys. Semicond. **15**, 1061 (1981).
[12] D. Polvani, J. Meng, N. Chandra Shekar, J. Sharp, and J. Badding, Chem. Mater. **13**, 2068 (2001).
[13] G. Zhang and Y.-W. Zhang, Mech. Mater. **91**, 382 (2015).
[14] L. Alghara gholy, T. Pope, and C. Lambert, J. Phys.: Condens. Matter **30**, 105304 (2018).
[15] H. Y. Lv, W. J. Lu, D. F. Shao, and Y. P. Sun, Phys. Rev. B **90**, 085433 (2014).
[16] R. G. Ross, P. Andersson, B. Sundqvist, and G. Backstrom, Rep. Prog. Phys. **47**, 1347 (1984).
[17] D. M. Darbha, in *Thermal Transport*, edited by P. G. Klemens and T. K. Chu (Springer, Boston, 1976).
[18] A. Beck, D. Darbha, and H. Schloessin, Phys. Earth Planet. Inter. **17**, 35 (1978).
[19] H. Yukutake and M. Shimada, Phys. Earth Planet. Inter. **17**, 193 (1978).
[20] Kh. I. Amirkhanov, Y. B. Magomedov, S. N. Emirov, and N. L. Kramynina, Sov. Phys.-Sol. St. **21**, 1619 (1979).
[21] A. Averkin, Z. Z. Zhaparov, and L. S. Stilbans, Sov. Phys. Semicond. **5**, 1954 (1972).
[22] W. Lu and C. M. Lieber, J. Phys. D: Appl. Phys. **39**, R387 (2006).
[23] R. Rurali, Rev. Mod. Phys. **82**, 427 (2010).
[24] J. Greil, A. Lugstein, C. Zeiner, G. Strasser, and E. Bertagnolli, Nano Lett. **12**, 6230 (2012).
[25] K. Winkler, E. Bertagnolli, and A. Lugstein, Nano Lett. **15**, 1780 (2015).
[26] H. Zhang, J. Tersoff, S. Xu, H. Chen, Q. Zhang, K. Zhang, Y. Yang, C.-S. Lee, K.-N. Tu, J. Li, and Y. Lu, Sci. Adv. **2**, e1501382 (2016).
[27] Z. L. Wang and J. Song, Science **312**, 242 (2006).
[28] S. Xu, Y. Qin, C. Xu, Y. Wei, R. Yang, and Z. L. Wang, Nat. Nanotechnol. **5**, 366 (2010).
[29] J. Zhou, Y. Gu, P. Fei, W. Mai, Y. Gao, R. Yang, G. Bao, and Z. L. Wang, Nano Lett. **8**, 3035 (2008).
[30] G. Lewis and C. Catlow, J. Phys. C: Solid State Phys. **18**, 1149 (1985).
[31] M. Nyberg, M. A. Nygren, L. G. M. Pettersson, D. H. Gay, and A. L. Rohl, J. Phys. Chem. **100**, 9054 (1996).
[32] D. Lide *et al.*, *Handbook of Chemistry and Physics*, 88th ed. (CRC Press, Boca Raton, FL, 2007).
[33] G. Fugallo and L. Colombo, Phys. Scr. **93**, 043002 (2018).
[34] Z. Fan, L. F. C. Pereira, H.-Q. Wang, J.-C. Zheng, D. Donadio, and A. Harju, Phys. Rev. B **92**, 094301 (2015).
[35] D. Demchenko and D. B. Ameen, Comput. Mater. Sci. **82**, 219 (2014).
[36] J. Che, T. Çağın, W. Deng, and W. A. Goddard III, J. Chem. Phys. **113**, 6888 (2000).
[37] L. Momenzadeh, B. Moghtaderi, I. V. Belova, and G. E. Murch, Comput. Condens. Matter **17**, e00342 (2018).
[38] W. Li, J. Carrete, N. A. Katcho, and N. Mingo, Comput. Phys. Commun. **185**, 1747 (2014).
[39] A. Togo and I. Tanaka, Scr. Mater. **108**, 1 (2015).
[40] P. Giannozzi, S. Baroni, N. Bonini, M. Calandra, R. Car, C. Cavazzoni, D. Ceresoli, G. L. Chiarotti, M. Cococcioni, I. Dabo *et al.*, J. Phys.: Condens. Matter **21**, 395502 (2009).
[41] P. Giannozzi, O. Andreussi, T. Brumme, O. Bunau, M. B. Nardelli, M. Calandra, R. Car, C. Cavazzoni, D. Ceresoli, M. Cococcioni *et al.*, J. Phys.: Condens. Matter **29**, 465901 (2017).
[42] J. P. Perdew, K. Burke, and M. Ernzerhof, Phys. Rev. Lett. **77**, 3865 (1996).
[43] M. Cococcioni and S. De Gironcoli, Phys. Rev. B **71**, 035105 (2005).

[44] X. Ma, B. Lu, D. Li, R. Shi, C. Pan, and Y. Zhu, J. Phys. Chem. C **115**, 4680 (2011).
[45] Y.-C. Peng, C.-C. Chen, H.-C. Wu, and J.-H. Lu, Opt. Mater. **39**, 34 (2015).
[46] H. J. Monkhorst and J. D. Pack, Phys. Rev. B **13**, 5188 (1976).
[47] D. Vanderbilt, Phys. Rev. B **41**, 7892 (1990).
[48] V. Srikant and D. R. Clarke, J. Appl. Phys. **83**, 5447 (1998).
[49] G. K. Madsen and D. J. Singh, Comput. Phys. Commun. **175**, 67 (2006).
[50] A. McGaughey and M. Kaviany, Int. J. Heat Mass Transfer **47**, 1799 (2004).
[51] G. Greene, Y. Cho, J. Hartnett, and A. Bar-Cohen, *Advances in Heat Transfer* (Elsevier Science, London, 2006), Vol. 39.
[52] J. Dong, O. F. Sankey, and C. W. Myles, Phys. Rev. Lett. **86**, 2361 (2001).
[53] X. Wu, J. Lee, V. Varshney, J. L. Wohlwend, A. K. Roy, and T. Luo, Sci. Rep. **6**, 22504 (2016).
[54] S. Bhowmick and V. B. Shenoy, J. Chem. Phys. **125**, 164513 (2006).
[55] K. Yuan, X. Zhang, D. Tang, and M. Hu, Phys. Rev. B **98**, 144303 (2018).
[56] J. A. Seijas-Bellido, H. Aramberri, J. Íñiguez, and R. Rurali, Phys. Rev. B **97**, 184306 (2018).
[57] R. Ghosh, D. Basak, and S. Fujihara, J. Appl. Phys. **96**, 2689 (2004).
[58] T. Ouyang and M. Hu, Phys. Rev. B **92**, 235204 (2015).